JOURNAL OF SPACECRAFT AND ROCKETS
Vol. 31, No. 5, September–October 1994

Base Drag Prediction on Missile Configurations

F. G. Moore*
Naval Surface Warfare Center, Dahlgren, Virginia 22448
F. Wilcox†
NASA Langley Research Center, Hampton, Virginia 23365
and
T. Hymer‡
Naval Surface Warfare Center, Dahlgren, Virginia 22448

New wind-tunnel data have been taken, and a new empirical model has been developed for predicting base drag on missile configurations. The new wind-tunnel data were taken at NASA Langley Research Center in the unitary wind tunnel at Mach numbers from 2.0 to 4.5, angles of attack to 16 deg, fin control deflections up to 20 deg, fin thickness-to-chord ratio of 0.05 to 0.15, and fin locations flush with the base to two chord lengths upstream of the base. The newly developed empirical model uses these data along with previous wind-tunnel data. It estimates base drag as a function of all the preceding variables along with boattail and power-on or power-off effects. In comparing the new empirical model to that used in the former aeroprediction code, the new model gives improved accuracy compared to wind-tunnel data. The new model also is more robust due to inclusion of additional variables. On the other hand, additional wind-tunnel data are needed to validate or modify the current empirical model in areas where data are not available.

Nomenclature

A = base area, in.^{2}
C_{A_B} = axial force coefficient due to base pressure
C_{D_B} = base drag coefficient, $(C_{A_B})_{\alpha=0}$
C_{P_B} = base pressure coefficient
c = fin chord, in.
d = body diameter at body base, in.
d_{ref} = reference diameter (body diameter), in.
F_1, F_2, F_3 = symbols defining parameters used in empirical model
M_∞ = freestream Mach number
p = freestream static pressure, lb/ft^2
p_i = measured static pressure, lb/ft^2
p_o = stagnation pressure, lb/ft^2
q = freestream dynamic pressure, lb/ft^2
R = radius of base, 2.5 in.
Re = Reynolds number, ft^{-1}
r = radius, in.
T_o = stagnation temperature, °F
t = fin thickness, in.
t/c = fin thickness-to-chord ratio
t/d = fin thickness-to-body reference diameter ratio
x = distance from body base to fin trailing edge (for $\delta = 0$ deg), in.
x/c = distance from body base to fin trailing edge (for $\delta = 0$ deg) in tail root chord lengths
α = body angle of attack, deg (positive nose up)
δ = fin control deflection, deg (positive leading edge up)

Subscripts on C_{P_B}

NF = C_{P_B} of body alone with no fins
t/c = C_{P_B} of body with fins of a given thickness-to-chord ratio
x/c = C_{P_B} of body with fins located a given distance from the body base in fin root chord lengths
α = C_{P_B} of body at a given angle of attack
δ = C_{P_B} of body with fins at a given deflection angle

Received April 20, 1993; revision received Aug. 23, 1993; accepted for publication Aug. 30, 1993.

*Senior Aerodynamicist, Weapons Systems Department, Dahlgren Division. Associate Fellow AIAA.
†Aerospace Engineer, High-Speed Aerodynamics Branch.
‡Aerospace Engineer, Aeromechanics Branch, Dahlgren Division.

Introduction

FOR the past 20 years, the Naval Surface Warfare Center, Dahlgren Division (NSWCDD) has been involved in developing codes to calculate aerodynamics on tactical weapons. These codes have attempted to meet the changing needs of the tactical weapons community and keep pace with aerodynamics requirements. A recent effort was undertaken to examine where we have been, where we are, and where we need to go in the future with respect to aerodynamics codes. One of the primary needs identified in Ref. 1 was an upgrade of the NSWCDD aeroprediction code to allow Mach numbers up to 20 (including the effects of real gases), improved lift prediction with particular emphasis on low-aspect ratio lifting surfaces, and improved base drag prediction. All three of these efforts were undertaken. This paper deals with the third of these, providing improved base drag prediction capability for missile configurations. Because base drag can account for as much as 40% of the total drag of some configurations at some conditions, it is an important part of the total drag.

The latest version of the aeroprediction code[2–4] (hereinafter referred to as old aeroprediction code or OAP) also calculates base drag empirically. It estimates the body-alone, zero angle-of-attack, power-off base drag using an average of wind-tunnel data presented in several references.[5–13] These data assume a long cylindrical afterbody with a fully developed turbulent boundary layer ahead of the base. Deviations to this assumption are expected due to Reynolds number, temperature, boattail or flare, angle of attack, fin t/c ratio, fin location, fin deflection, low body fineness ratio, or power-on.

The methodology of Refs. 2–4 neglects the effects of Reynolds number by assuming a Reynolds number combined with body roughness high enough to ensure fully developed turbulent flow at the base. Surface temperature effects are also neglected. The body is assumed to be at least 5–6 calibers long so that body fineness ratio effects are minimal. Also, fin deflection effects were not accounted for due to lack of data. The body-alone, angle-of-attack base pressure coefficient change was estimated from Ref. 7 using limited data at very low angle of attack. The effects due to fin t/c ratio and fin location were estimated using the meager amount of data

from Refs. 14–16. Below $M_\infty = 1.5$, the effects were extrapolated to $M_\infty = 0$ based on judgment and some test data on configurations where the effects of fins could not clearly be separated from other effects.

Finally, power-on effects were estimated by modifying the methodology of Brazzel[17,18] for higher values of mass flow at nozzle exit. Also, boattail effects were estimated by the empirical data of Stoney.[12] For details of the methodology and equations used, the interested reader is referred to Refs. 19 and 20.

There are several problems with the methodology used in the OAP. All of these stem from the limited wind-tunnel data available to estimate the change in base pressure as a function of the key parameters of interest. For most tactical missiles, it is believed that the neglect of Reynolds number, surface temperature, and body length-to-diameter ratio effects are acceptable so long as one remembers the constraints on which these assumptions are made. Also, it is believed that the methodology in the OAP for inclusion of boattail and power-on effects is acceptable at present. However, estimates of the change in base pressure due to angle of attack, fin thickness, fin deflection, and fin location need to be improved on or accounted for.

More specifically the data for angle-of-attack effects were limited to small angles of attack ($\leq$10 deg) and Mach number ($1.5 \leq M_\infty \leq 2.4$). The data for fin location and t/c ratio was limited to $0 \leq x/c \leq 2.0$ and $0 \leq t/c \leq 0.10$. It is well known that as Mach number gets high, base drag goes to zero. Hence, it is desirable to have base pressure measurements for $M_\infty < 5.0$; $\alpha \leq 30$ deg; $t/c \leq 0.15$; $x/c \leq 2.0$; and $\delta \leq 20$ deg. Also, data where a combination of these variables is investigated simultaneously are needed. Using these data, a more comprehensive empirical model to estimate base drag on missile configurations can be developed. Although the data are needed for an improved base drag prediction model, they could also be useful in validating Navier Stokes codes and selecting appropriate turbulence models.

As a result of the need for additional wind-tunnel test data, a request was made to NASA Langley Research Center (NASA/LaRC) to assist in providing such data. The data taken to date are for $2.0 \leq M_\infty \leq 4.5$, $\alpha \leq 16$ deg, $\delta \leq 20$ deg, $t/c \leq 0.15$, and $x/c \leq 2.0$. Although these data are not as extensive as desired, they are by far the most extensive base drag database to date and will help in refining the empirical base drag prediction model of Refs. 19 and 20. It is hoped that additional data at lower Mach numbers and higher angles of attack will be obtained in the future for additional refinements. This paper summarizes the new base drag wind-tunnel test results and derives an improved empirical base drag prediction model based on these and other wind-tunnel results.

Experimental Tests

Model and Tunnel Description

A drawing of the missile base pressure model along with the location of base pressure taps is shown in Fig. 1. The missile body was an ogive cylinder 36 in. long and 5.0 in. in diameter. Four cruciform aft tail fins could be attached to the missile body in a plus orientation at three longitudinal locations. These locations included flush with the base and one and two root-chord lengths ahead of the base. At each longitudinal location, the fin incidence could be set at 0, 10, and 20 deg. Three sets of fins were tested that had the same planform but varied in thickness. The airfoil of the fins was a double wedge with sharp leading and trailing edges. Three t/c ratios were tested including $t/c = 0.05, 0.1, 0.15$ (interested readers are referred to Ref. 21 for further details of the model). The base was instrumented with 89 pressure orifices arranged along radial lines at 22.5 deg increments and 7 constant radiuses from the center of the base.

The model was attached to a vertical strut near the middle of the missile body on the upper surface (leeward side of model as α increases). The strut had a diamond cross section and was swept 15 deg. The strut leading-edge wedge half-angle was 12 deg and was sufficiently small to maintain an attached shock on the leading edge at the lowest Mach number tested and at small angles of attack. At larger angles of attack, the strut was on the leeward side of the missile body and would have minimal influence on the missile base pressure. The top of the strut was sufficiently far from the model centerline (19.25 in.) so that a Mach line emanating from the top leading edge of the strut would not intersect a tail fin on the model and would intersect the model centerline at least 1.5 body diameters downstream of the model base at the lowest Mach number tested. The strut was attached to the tunnel model support system through a 90 deg-offset sting holder that allowed the vertical position of the model to be varied in the tent section. The model nose was typically slightly below the tunnel centerline to increase the maximum attainable angle of attack and provide clearance at the tunnel ceiling to ensure that the strut was outside of the tunnel wall boundary layer to minimize possible boundary-layer separation and tunnel-flow breakdown.

The wind-tunnel tests were conducted in the NASA/LaRC Unitary Plan Wind Tunnel (UPWT), which is a continuous flow, variable pressure supersonic wind tunnel with a Mach number range of 1.5–4.6. The tunnel has two test sections, each of which covers only part of the Mach number range; the low Mach number test section has a range of 1.5–2.9, and the high Mach number test section has a range of 2.4–4.6. The test sections are approximately 4 ft square by 7 ft long. The nozzle ahead of each test section consists of an asymmetric sliding block that allows a continuous variation of Mach number while the tunnel is in operation. A complete description of the tunnel and test section calibration information is presented in a

Table 1 Test conditions

M_∞	Re	p_o	T_o	q
2.0	2×10^6	1253	125	449
2.5	2×10^6	1600	125	410
3.0	2×10^6	2216	150	380
3.5	2×10^6	2882	150	324
4.0	2×10^6	3698	150	273
4.5	2×10^6	4666	150	229

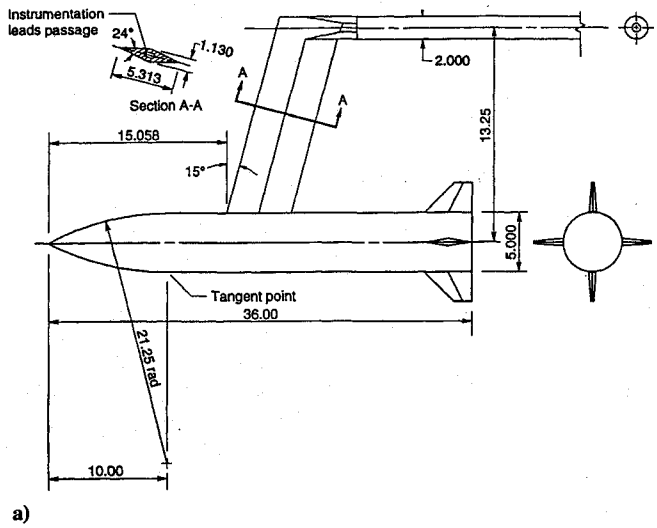

a)

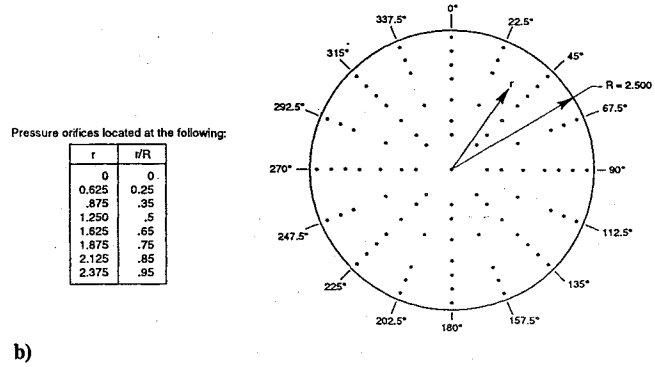

b)

Fig. 1 Missile base pressure model description (linear dimensions in in.): a) body support strut details and b) base pressure orifice locations.

Table 2 Configuration index

Configuration	Fins off	t/c			x/c			δ			$\alpha(M_\infty = 2.0)$	$\alpha(M_\infty \geq 2.5)$
		0.05	0.10	0.15	0	1.0	2.0	0	10	20		
1	x	—	—	—	—	—	—	—	—	—	Sweep	Sweep
2	—	—	—	x	x	—	—	x	—	—	0, 5, 10	0
3	—	—	—	x	x	—	—	—	x	—	0, 5, 10	0
4	—	—	—	x	x	—	—	—	—	x	0, 5, 10	0
5	—	—	x	—	x	—	—	x	—	—	0, 5, 10	0
6	—	—	x	—	x	—	—	—	x	—	0, 5, 10	0
7	—	—	x	—	x	—	—	—	—	x	0, 5, 10	0
8	—	x	—	—	x	—	—	x	—	—	0, 5, 10	0
9	—	x	—	—	x	—	—	—	x	—	0, 5, 10	0
10	—	x	—	—	x	—	—	—	—	x	0, 5, 10	0
11	—	x	—	—	—	x	—	x	—	—	0, 5, 10	0
12	—	—	x	—	—	x	—	x	—	—	0, 5, 10	0
13	—	—	—	x	—	x	—	x	—	—	0, 5, 10	0
14	—	—	—	x	—	—	x	x	—	—	0, 5, 10	0
15	—	—	x	—	—	—	x	x	—	—	0, 5, 10	0
16	—	x	—	—	—	—	x	x	—	—	0, 5, 10	No data

Table 3 Example of average base pressure coefficient data

Configuration	M_∞	α	$-C_{P_B}$
1	2.5	0.0	0.106
1	2.5	2.0	0.119
1	2.5	4.0	0.136
1	2.5	6.0	0.148
1	2.5	8.0	0.157
1	2.5	10.0	0.165
1	2.5	12.0	0.160
1	2.5	14.0	0.156
1	2.5	15.0	0.154
1	2.5	15.8	0.149

NASA report.[22] The tests were conducted at the conditions shown in Table 1.

The model angle of attack was varied from 0 deg to approximately 16 deg for tests conducted in the high Mach number test section ($M_\infty \geq 2.5$) and from 0 deg to approximately 10 deg for tests conducted in the low Mach number test section ($M_\infty = 2.0$).

To ensure a turbulent boundary layer over the model, transition grit was applied to the missile nose and to the leading edge of each fin. The transition strips were located 1.8 in. from the model nose measured along the model surface and 0.6 in. from the fin leading edges measured streamwise. The size and location of the transition grit was determined from documented procedures[23] except that a critical roughness Reynolds number of 1800 was used instead of the recommended value of 600. The increase in critical roughness Reynolds number above the recommended value was due to the effects of high Mach number and was determined using guidance from a NASA publication[24] and unpublished data obtained in the UPWT.

Measurements and Data

The pressures on the model were measured with two electronically scanned pressure modules that were located inside the model. The modules had a full-scale range of ±5 psid. All 89 pressure orifices on the model base were measured simultaneously for each data point. The model angle of attack was measured with an accelerometer that was mounted inside the missile body. The missile base drag coefficient was calculated using an area weighted average of the base pressure coefficients.

Tests were conducted both with and without tail fins. Data were obtained at discrete α for cases with tail fins and over a range of α for cases without tail fins. A complete description of all the configurations that were tested is contained in Table 2. Table 3 contains a sample of the data taken for configuration 1 of Table 2 at $M_\infty = 2.5$. For more details of the test data, as well as the new empirical model, the interested reader is again referred to Ref. 21.

Two problems arose during this test that affected the uncertainty of the measured pressure data using the electronically scanned pressure modules. The first problem was model vibrations, which were possibly caused by either normal tunnel vibrations being transmitted through the long-cantilevered sting/strut or aerodynamic flow unsteadiness that caused the model and sting/strut to vibrate. The model was not instrumented to determine the exact cause of the vibrations. The second problem was temperature variations inside the model that were primarily caused by the variation of tunnel stagnation temperature as the tunnel was brought online to the desired test conditions. Because no data were specifically obtained to determine the experimental data uncertainty caused by model vibrations and temperature variations, the pressure data uncertainty was estimated from data obtained during routine checks of the pressure instrumentation to ensure data system integrity. The checks consisted of either applying a known pressure to the modules on all the pressure ports and comparing the module reading to a standard pressure gauge, or calibrating the module on-line[25] and comparing data points taken before and after the calibration. Using the data from these checks, the base drag coefficients are estimated to have an uncertainty of approximately ±5% of the calculated values.

Empirical Model for Base Drag Prediction

Body-Alone Configuration

Using the new wind-tunnel data of Ref. 21 along with the data generated[26] since the OAP base drag model was developed, a new body-alone, zero angle-of-attack base pressure coefficient model was generated. This model is presented in Fig. 2 as the improved aeroprediction (IAP) curve and compared to the former aeroprediction code (OAP). The results differ slightly with the IAP being slightly lower than the OAP for $M_\infty > 3$ and slightly higher for $M_\infty < 1.5$.

Using the wind-tunnel data of Ref. 21 (a sample of which is shown in Table 3), the percent change in the body-alone base pressure co-

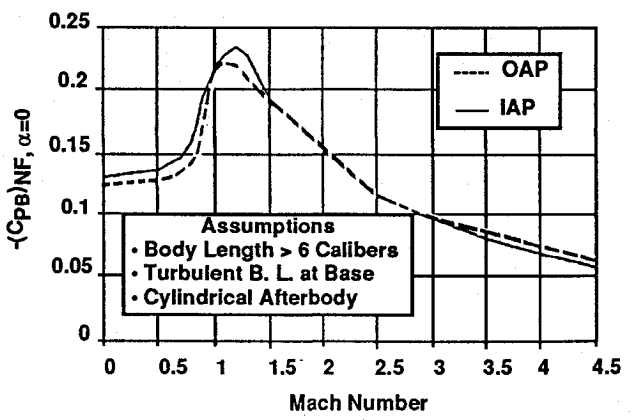

Fig. 2 Mean body-alone base pressure coefficient used in OAP and IAP.

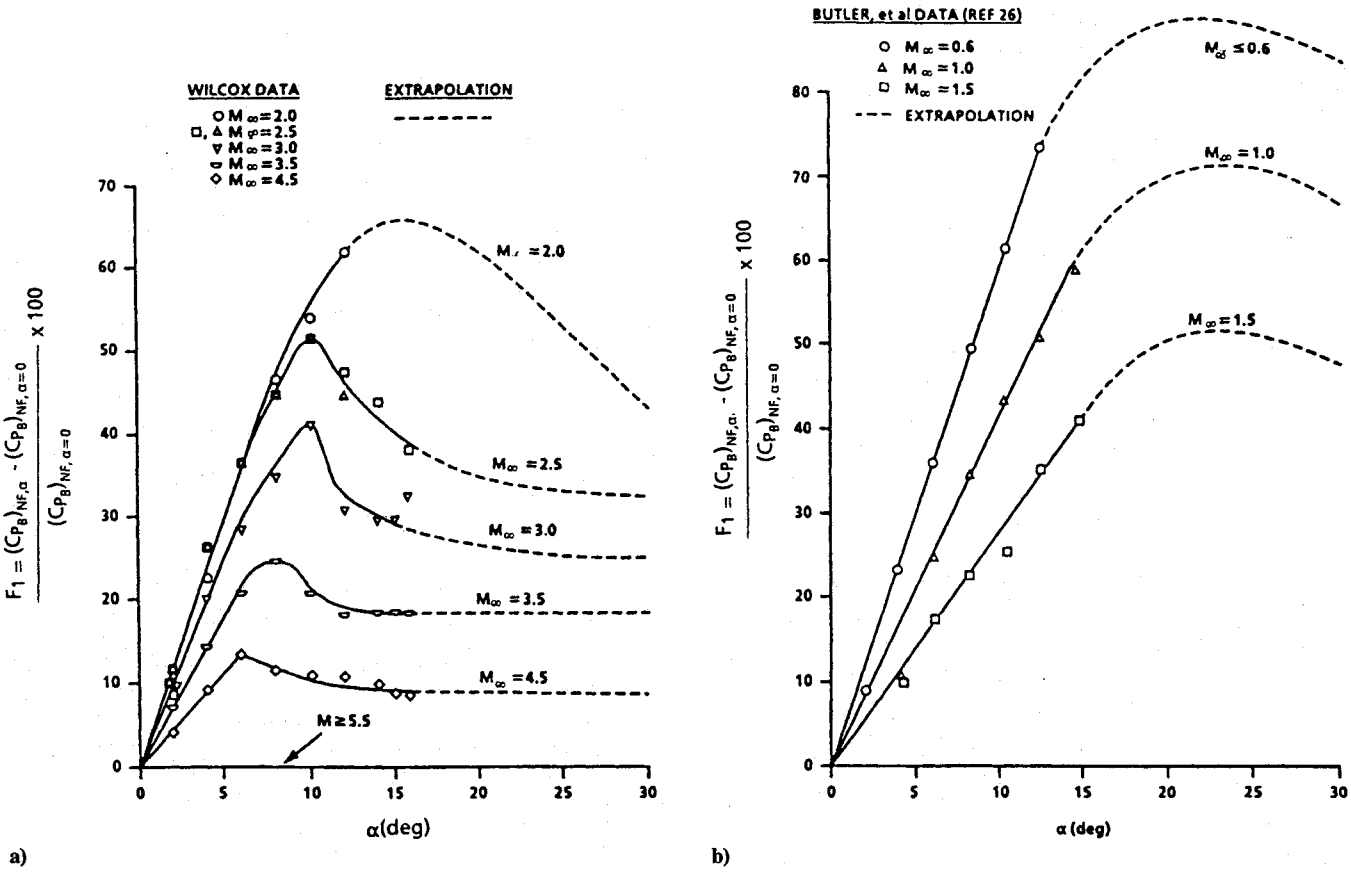

Fig. 3 Percent increase in body-alone base pressure coefficient due to angle of attack: a) $M_\infty \geq 2$ and b) $M_\infty < 2$.

efficient was calculated as a function of angle of attack, and these results are given in Fig. 3a for Mach numbers $2.0 \leq M_\infty \leq 4.5$. Note that no data are available above $M_\infty > 4.5$, so a linear extrapolation indicates no change in base pressure with angle of attack above $M_\infty = 5.5$. Also, no data could be taken for angles of attack greater than about 15 deg because the model support would have hit the tunnel ceiling. For higher angles of attack, the data for $M_\infty \geq 2.5$ show an angle of attack where the base pressure increase is a maximum and then a gradual decline with further increases in α. This general trend was assumed for all results in both Figs. 3a and 3b until additional high angle-of-attack data are made available. The large unpublished NASA Tri Service Data Base was investigated for inclusion of high angle-of-attack pressure effects. However, the emphasis in those tests was on lifting properties, and the axial force was of secondary concern. Hence, although axial force and base pressure information is available, the accuracy of the base pressure information is not believed to be as good as desired for use here.

For Mach numbers below 2, data of Ref. 26 were used to obtain the change in base pressure due to angle of attack. These results are given in Fig. 3b. In contrast to the Tri Service Data Base, this test did concentrate on axial force information. The Reynolds number of the transonic portion of the test was also high enough to ensure a turbulent boundary layer at the base for Mach numbers less than 1.5. However, only three base pressure taps were mounted on the base of the model, and a sting was also in place. Hence, the data are probably not of the same quality as that of the more recent data in Ref. 21 and summarized in this paper, where numerous pressure taps were available to get a more accurate average of base pressure.

It should be pointed out that both Figs. 3a and 3b are given in percent change in the body-alone base pressure coefficient as a function of angle of attack. These curves were obtained using data from Ref. 21 and Fig. 2 for $2.0 \leq M_\infty \leq 4.5$ and Ref. 26 and Fig. 2 for $0.6 \leq M_\infty < 2.0$. The quantity F_1 was calculated by subtracting the body-alone value of C_{P_B} at $\alpha = 0$ deg (from Ref. 21 or 26) from the body-alone value of C_{P_B} at some α (from Ref. 21 or 26) and dividing this quantity by the body-alone value of C_{P_B} at $\alpha = 0$ deg from Fig. 2. This method of nondimensionalizing the change in C_{P_B} of the present experimental data with the C_{P_B} at $\alpha = 0$ deg from Fig. 2 compensates for the slight difference between the body-alone value C_{P_B} at $\alpha = 0$ deg from Fig. 2 and Ref. 21 or 26. It should be emphasized that throughout this section describing the derivation of the empirical base drag prediction model, the body-alone value of C_{P_B} at $\alpha = 0$ deg $[(C_{P_B})_{NF,\alpha=0}]$ used to nondimensionalize the changes in the present experimental data was obtained from Fig. 2.

In viewing Figs. 3a and 3b, it is evident that angle of attack has a strong effect on base pressure and hence base drag. It is also evident that additional wind-tunnel data are needed for angles of attack greater than 15 deg at $M_\infty \leq 4.5$.

The base pressure coefficient and drag of the body-alone configuration is then estimated as

$$(C_{P_B})_{NF,\alpha} = (C_{P_B})_{NF,\alpha=0}[1 + 0.01F_1] \tag{1}$$

and

$$C_{A_B} = (-C_{P_B})_{NF,\alpha}(d/d_{\text{ref}})^3 \tag{2}$$

where $(C_{P_B})_{NF,\alpha=0}$ comes from the IAP results of Fig. 2 and F_1 from Figs. 3a and 3b. Note that the d/d_{ref} of Eq. (2) is cubed rather than squared to account for boattail effects according to Ref. 12. Equation (2) is the model used in the OAP[19] to estimate boattail effects, and it is the same model that will be used in the IAP.

Body-Tail Configuration

There are three significant base pressure effects that need to be accounted for on missiles having tail surfaces located near the base. These include fin deflection, fin thickness, and fin location. Fin planforms shape and aspect ratio also are design parameters of interest. However, they will not be modeled in the present empirical methodology. As seen in the previous discussion on the wind-tunnel test, a double-wedge airfoil section was used for all tests. The fin planform had a constant aspect ratio of 1.82, and the fin trailing edges were sharp. The planform shape chosen was thus fairly typical of missile tail fin planforms both in aspect ratio and airfoil section.

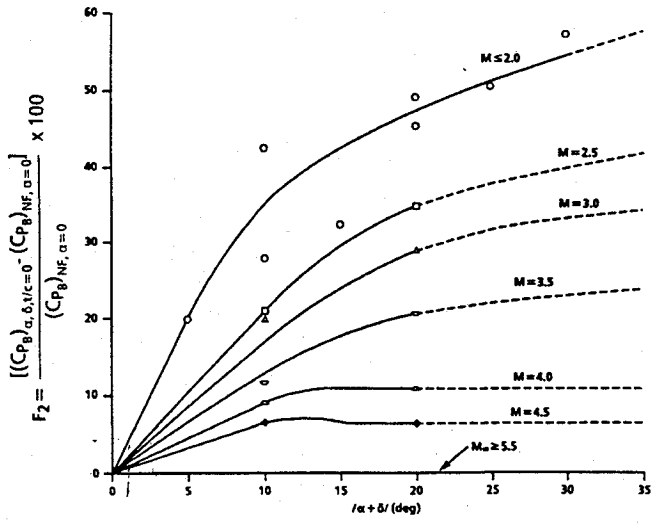

Fig. 4 Percent increase in base pressure coefficient due to combined effects of angle of attack and control deflection; $t/c \approx 0, x/c \approx 0$.

The first effect to consider is control deflection. Initially, it was hoped that body angle of attack and fin control deflection could be separated and modeled separately. However, it became clear that this was not possible for two reasons:

1) More data were needed than were acquired in the test.

2) Based on the limited amount of data available, it appeared that angle of attack and control deflection were closely coupled.

As a result, when fins were present, the empirical model arrived at a curve that gave the percent increase in base pressure coefficient as a function of the absolute value of $\alpha + \delta$ based on the limited amount of data available. To arrive at this curve, it was first necessary to determine the increase in base pressure due to fin deflection for zero thickness fins. This was done by taking the data for the three values of t/c available and extrapolating to $t/c = 0$. Fig. 4 presents the entire data set of increase in base pressure at $t/c = 0$ as a function of $|\alpha + \delta|$. Here, the figure has been nondimensionalized by the value of the body-alone base pressure coefficient and given as a percentage increase. A linear extrapolation of the data above $M_\infty = 4.5$ indicates that there is no increase at $M_\infty = 5.5$. However, no accurate data are known to be available for $M_\infty < 2$, so the curve for $M_\infty = 2$ is assumed to hold below $M_\infty = 2$. It should be pointed out that this is one reason that the empirical model was derived in terms of percent increase in base pressure coefficient relative to the body-alone base pressure coefficient at $\alpha = 0$. This way, although no data for control deflection effects are available below $M_\infty = 2$, we still know $(C_{P_B})_{NF,\alpha=0}$ fairly accurately for the body alone; hence, it is believed that the assumption of using the curve in Fig. 4 to represent the percent increase in base pressure due to fin deflection is better than trying to derive a model based on the value of ΔC_{P_B} due to fin deflection. The only assumption in Fig. 4, therefore, is the shape of the curve at $M_\infty = 2$ is assumed to apply below $M_\infty = 2$.

It is apparent from Fig. 4 that additional wind-tunnel data are needed for control deflection and body angle of attack below $M_\infty = 2$ as well as combined values of $|\alpha + \delta|$ at $M > 2$ in order to have a more accurate estimate of percent increase in base pressure coefficient due to control deflection. However, until additional data become available, Fig. 4 will be the model used in the IAP.

The next parameter of interest is fin thickness effects on base pressure. Most references (see, e.g., Refs. 14 and 15), including the OAP model, estimate the change in base pressure as a function of fin t/c ratio. However, in plotting data from several sources, it appeared that t/c may not be the most appropriate parameter. Fin t/d was also investigated and this appeared to be a much more appropriate way to approximate fin thickness. As a result, the empirical model of fin thickness effects on base pressure is derived on the basis of t/d vs t/c.

In analyzing the data of the present report, it also became clear that fin thickness was an important parameter at low angle of attack and control deflection but became less important at larger values of $|\alpha + \delta|$. That is, given the increase of C_{P_B} due to $|\alpha + \delta|$ from Fig. 4,

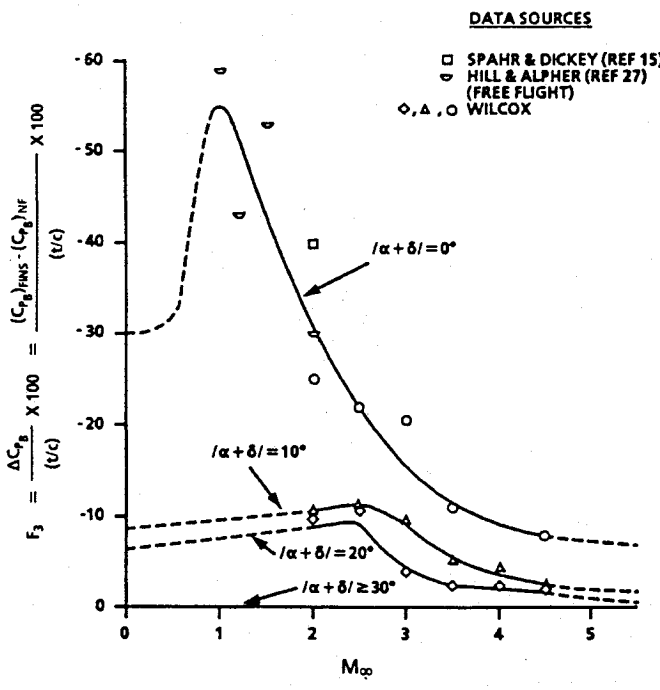

Fig. 5 Additional percent change in base pressure coefficient due to fin thickness at various values of $|\alpha + \delta|$.

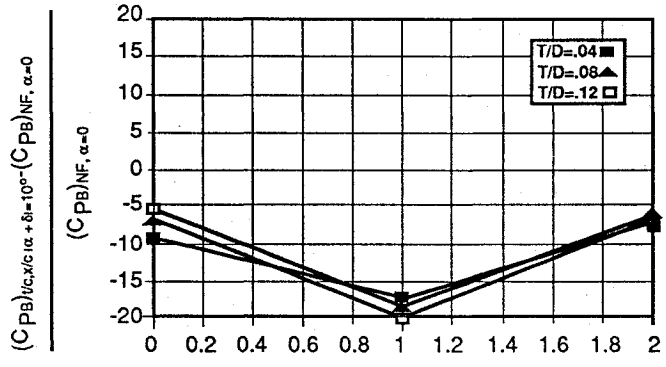

Fig. 6 Percent change in base pressure coefficient due to fin location; $|\alpha + \delta| = 10$ deg, $M_\infty = 2.0$.

the additional change in C_{P_B} due to fin thickness decreased with increasing $|\alpha + \delta|$. These results are shown in Fig. 5, which gives the additional percent change in base pressure due to fin t/d ratio as a function of Mach number and $|\alpha + \delta|$. Once again, additional data are needed, in particular for Mach numbers less than 2. For $|\alpha + \delta| = 0$, the data of Ref. 27 supplement the present data down to $M_\infty = 1.0$. Until additional data are available, the trend of F_3 below $M_\infty = 1$ is assumed to be similar to that of the base pressure coefficient curve of Fig. 2. Also, for values of $|\alpha + \delta| \geq 30$ deg, fin thickness effects on base pressure are assumed to be zero.

The total body base pressure coefficient for fins located flush with the base is then

$$(C_{P_B})_{\alpha,\delta,t/c,x/c=0} = [1 + 0.01F_2](C_{P_B})_{NF,\alpha=0} + 0.01F_3(t/d) \quad (3)$$

where $(C_{P_B})_{NF,\alpha=0}$, F_2, and F_3 come from the IAP curve of Fig. 2 and Figs. 4 and 5, respectively.

The final parameter to model is fin location effects relative to the body base. Figure 6 shows the percent change in base pressure coefficient for 10 deg angle of attack and various t/d values as a function of x/c for $M_\infty = 2$. This figure was based entirely on the new wind-tunnel data of Ref. 21. Note that the ΔC_{P_B} of Fig. 6 is the change in base pressure at a given angle of attack due to the presence of the fins. Examining Fig. 6, it is seen that as α or $|\alpha + \delta|$ becomes appreciable, the fins need to be located about 2.5 calibers ahead of the base before the fin effects are minimal and the body angle-of-attack effect is the dominant factor.

Also, it is noted that the percent change in base pressure coefficient in Fig. 6 initially has a negative slope but then reverses and approaches no change at $x/c = 2.5$. As a result, a numerical interpolation is used to compute the percent change in ΔC_{P_B} as a function of x/c, $|\alpha + \delta|$, and t/d. This same percent change is assumed to occur at all Mach numbers because no data are available other than at $M_\infty = 2$. However, Ref. 21 does show data for $\alpha = 0$ and 5 deg.

Once the percent change in C_{P_B} due to the presence of the fins has been determined from Fig. 6, the total C_{P_B} is then,

$$(C_{P_B})_{\alpha,\delta,t/c,x/c} = (C_{P_B})_{NF,\alpha} + 0.01(\Delta C_{P_B})_{\alpha,\delta,t/c,x/c} \qquad (4)$$

Here $(C_{P_B})_{NF,\alpha}$ is the body-alone base pressure coefficient at a given angle of attack and ΔC_{P_B} is the change due to the effect of fins from Fig. 6. Note that $(C_{P_B})_{NF,\alpha}$ is calculated by Eq. (1). As a result, the effect due to fins and body angle of attack will change from that due to fins in presence of the body when the fins are flush with the base to that of the body alone at angle of attack when the fins are far enough upstream. Power-on and boattail effects will modify this base pressure coefficient the same as previously discussed.

To summarize the fin location effects, if x/c is close to zero, Eq. (3) is used to compute the fin effect on base pressure. If $x/c \neq 0$, a numerical interpolation is used based on Fig. 6 where the variables are x/c, t/d, and $|\alpha + \delta|$. The body-alone angle-of-attack effect is computed by Eq. (1). The fin effects on base pressure vary from the values of Eq. (3), where $x/c = 0$ to those of the body-alone Eq. (1) upstream of the base. The total power-off base pressure coefficient is then given by Eq. (4). The base pressure coefficient is modified for power-on effects as currently done in the OAP. The base axial force coefficient including boattail effects is then

$$C_{A_B} = (-C_{P_B})_{\alpha,\delta,t/c,x/c}(d/d_{\text{ref}})^3 \qquad (5)$$

Comparison of Base Drag Empirical Models to Wind-Tunnel Data

This section compares the improved empirical base drag prediction model (IAP) with the older methodology currently in use in the 1981 version of the aeroprediction code. The data used are those of the present tests plus those of Ref. 26 for low Mach number body-alone angle-of-attack effects.

Figure 7 is an example (see Ref. 21 for other results) of the IAP and OAP prediction results for body-alone angle-of-attack base pressure for two Mach numbers. The IAP results show improvement over the OAP prediction at all Mach numbers. However, the OAP model, although it was based on a sparse amount of data, exhibits the correct trends and is reasonably accurate. The maximum error on C_{P_B} compared to the data for the OAP was about 20%. Of course, the IAP model duplicates the wind-tunnel results, just as it was designed to do.

Figure 7 further illustrates the fact that the empirical models of the OAP and IAP basically guess as to the behavior of base pressure

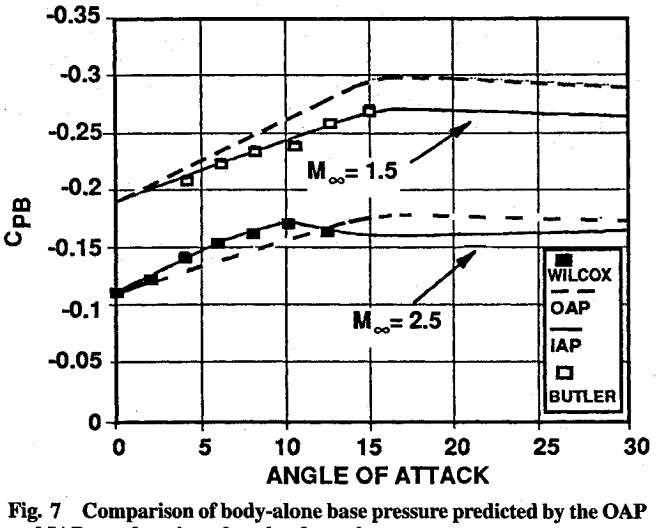

Fig. 7 Comparison of body-alone base pressure predicted by the OAP and IAP as a function of angle of attack.

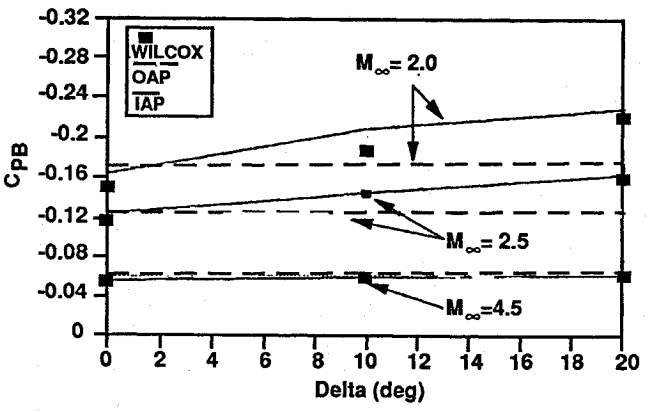

Fig. 8 Comparison of body-tail base pressure predicted by the OAP and IAP as a function of control deflection; $t/c = 0.05, x/c = 0$.

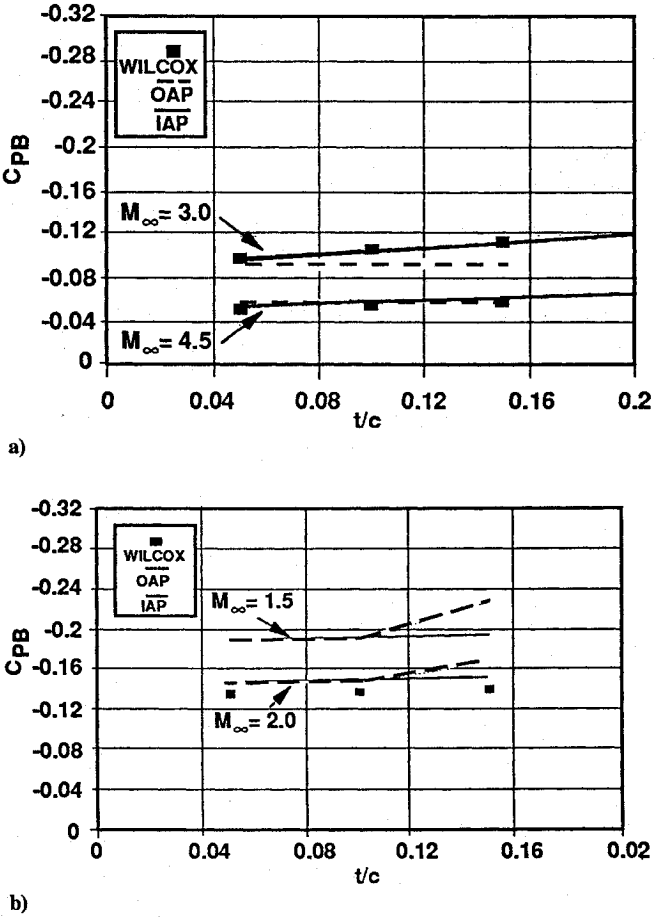

Fig. 9 Comparison of body-tail base pressure predicted by the OAP and IAP as a function of fin thickness: a) $\alpha = \delta = 0, x/c = 0$ and b) $\alpha = \delta = 0, x/c = 1.0$.

above $\alpha = 15$ deg due to lack of a reliable database. This guess is believed good at $M_\infty \geq 3.5$ but questionable for lower Mach numbers. On the other hand, it is certainly better than assuming no change in base pressure with angle of attack, which is what many engineering codes assume.

As already discussed, when there is a tail located in the vicinity of the base, the base pressure is affected due to several parameters. Figure 8 shows an example of the IAP computations for C_{P_B} as a function of δ compared to the results of the present test data of Wilcox. Also shown are the OAP results, which are straight lines because the OAP empirical model does not include δ as one of its parameters. Figure 8 is for $t/c = 0.05$ and $x/c = 0$. Note that at all Mach numbers (other than $M_\infty = 2$), the IAP represents the available data reasonably well. At $M_\infty = 2$, the empirical model

intentionally is slightly higher than the current experimental data for two reasons. First, to use the data of the current tests would cause the IAP curve of Fig. 2 to be unsmooth. Second, it is suspected that the values of the present test may be slightly on the low side, as compared to the OAP curve of Fig. 2, which represents a compilation of experimental data from other sources.

Figure 9 compares the base pressure coefficient of the OAP and IAP as a function of t/c for $x/c = 0$ and 1.0 and at several Mach numbers. Data of Ref. 21 are shown where available. It is clear in Fig. 9 that the IAP is superior to the OAP when compared to data for values of the various parameters where data are available. For Mach numbers where data are lacking, it is suspected that the present model is also superior. However, additional data are required to substantiate this.

Summary and Recommendations

To summarize, new wind-tunnel data have been generated to aid in base pressure prediction as a function of body angle of attack, Mach number, fin control deflection, fin thickness, and fin location. Data were taken over a Mach number range of 2–4.5, angle of attack of 0–16 deg, fin t/c ratio of 0.05 to 0.15, fin location of flush with the base to two chord lengths ahead of the base, and control deflection of 0–20 deg. At Mach 2, some data were taken with a combination of several of the preceding variables present; whereas, at other Mach numbers, only one parameter was changed for a given tunnel condition.

Based on these new data, more recent data from other wind-tunnel tests conducted since the empirical base drag model for the OAP was developed in the mid-1970s, and the data from which the empirical model was originally developed, a new and improved empirical base drag prediction model has been developed. This new model is a function of Mach number, angle of attack, fin control deflection, fin thickness, and fin location. In comparison with the OAP and the new wind-tunnel data set, it is seen that the IAP reduces the errors of the OAP substantially. Furthermore, the OAP did not account for fin deflection or even angle-of-attack effects if tail fins were present.

Although the new model estimates angle-of-attack effects to 30 deg, control deflection up to 30 deg, and fin thickness effects for all Mach numbers, in many cases these estimates are based on extrapolations and engineering judgment. As a result, additional wind-tunnel data are needed to validate or modify the current model as appropriate. In particular, it is recommended that data be taken for base pressure for the following conditions:

1) body alone: $15 \leq \alpha \leq 30$ deg; $0 \leq M_\infty \leq 4.5$

2) body tail: fins flush with base; 15 deg $\leq \alpha \leq 30$ deg; $M_\infty \leq 4.5$

3) body tail: fins flush with base; $\alpha = 0$; $0.05 \leq t/c \leq 0.15$; $0 \leq M_\infty < 2.0$

4) body tail: fins upstream of base; several values of α and δ; one value of t/c; three Mach numbers

5) body tail: more cases where combinations of several parameters are tested simultaneously for use in an empirical model validation

All data taken in future tests should be taken with the same rigor as in the present tests where enough pressure taps are used to get a good average of base pressure for use in base drag computations.

Acknowledgments

Appreciation is expressed to NASA Langley Research Center for its support in designing, building, and testing the wind-tunnel model used for obtaining additional wind-tunnel data. Acknowledgments are also given to Jim Bible and Sam Hardy of the Aeromechanics Branch, who provided some of the earlier wind-tunnel model design ideas and wind-tunnel test consultation. The empirical base drag methodology developed in this paper, along with partial cost of the wind-tunnel model, was provided through the Office of Naval Research (Dave Siegel) and, more specifically, the Surface-launched Weapons Technology Block Program managed at the Naval Surface Warfare Center, Dahlgren Division, by Robin Station. Appreciation is expressed to these individuals for their support of this work.

References

[1]Moore, F. G., "Computational Aerodynamics at NAVSWC: Past, Present, and Future," Naval Surface Warfare Center, NAVSWC TR 90-569, Dahlgren, VA, Oct. 1990.

[2]Devan, L., "Aerodynamics of Tactical Weapons to Mach Number 8 and Angle of Attack 180 deg: Part I, Theory and Application," Naval Surface Warfare Center, NSWC TR 80-346, Dahlgren, VA, Oct. 1980.

[3]Devan, L., and Mason, L., "Aerodynamics of Tactical Weapons to Mach Number 8 and Angle of Attack 180 deg: Part II, Computer Program and Users Guide," Naval Surface Warfare Center, NAVSWC TR 81-358, Dahlgren, VA, Sept. 1981.

[4]Devan, L., Mason, L., and Moore, F. G., "Aerodynamics of Tactical Weapons to Mach Number 8 and Angle of Attack 180 deg," AIAA Paper 82-0250, Jan. 1982.

[5]Love, E. S., "Base Pressure at Supersonic Speeds on Two-Dimensional Airfoils and on Bodies of Revolution with and without Turbulent Boundary Layers," NACA TN 3819, Jan. 1957.

[6]Chapman, D. R., "An Analysis of Base Pressure at Supersonic Velocities and Comparison with Experiment," NACA TR 1051, 1951.

[7]Bureau of Naval Weapons, "Handbook of Supersonic Aerodynamics," NAVWEPS Rept. 1488, Vol. 3, Oct. 1961.

[8]Reller, J. O., Jr., and Hamaker, F. M., "An Experimental Investigation of the Base Pressure Characteristics of Nonlifting Bodies of Revolution at Mach Numbers from 2.73 to 4.98," NACA TN 3393, March 1955.

[9]Peck, R. F., "Flight Measurements of Base Pressure on Bodies of Revolution With and Without Simulated Rocket Chambers," NACA TN 3372, April 1955.

[10]Fraenkel, L. E., "A Note on the Estimation of the Base Pressure on Bodies of Revolution at Supersonic Speeds," Royal Aircraft Establishment TN/AERO 2203, 1952.

[11]U.S. Army Missile Command, "Engineering Design Handbook: Design of Aerodynamically Stabilized Free Rockets," U.S. Army Material Command, AMCP-706-280, Washington, DC, July 1968.

[12]Stoney, W. E., Jr., "Collection of Zero-lift Data on Bodies of Revolution from Free-Flight Investigations," NASA TR R-100, 1961.

[13]Kurzweg, H. H., "New Experimental Investigations on Base Pressure in the NOL Supersonic Wind Tunnels at Mach Numbers 1.2 to 4.24," NOL Memo 10113, 1950.

[14]Heyser, A., Maurer, F., and Oberdorffer, E., "Experimental Investigation on the Effect of Tail Surfaces and Angle-of-Attack on Base Pressure in Supersonic Flow," *Conference Proceedings: The Fluid Dynamic Aspects of Ballistics*, AGARD-CP-10, 1966, pp. 263–290.

[15]Spahr, J. R., and Dickey, R. R., "Effect of Tail Surfaces on the Base Drag of a Body of Revolution at Mach Numbers of 1.5 and 2.0," NACA TN-2360, April 1951.

[16]Hill, F. K., and Alpher, R. A., "Base Pressures at Supersonic Velocities," *Journals of Aeronautical Sciences*, Vol. 16, No. 3, 1949, pp. 153–160.

[17]Brazzel, C. E., and Henderson, J. H., "An Empirical Technique for Estimating Power-On Base Drag of Bodies-of-Revolution with a Singe Jet Exhaust," *Proceedings, Specialists Meeting Sponsored by the AGARD Fluid Dynamics Panel*, Mulhouse, France, 5–8 Sept. 1966.

[18]Johnson, L. H., "Approximate Engine-on Base Pressure Computations for Aerodynamic Computer Codes," Naval Surface Warfare Center, NSWC K21 TM 82-11, Dahlgren, VA, March 1982.

[19]Moore, F. G., "Body Alone Aerodynamics of Guided and Unguided Projectiles at Subsonic, Transonic, and Supersonic Mach Numbers," NWL TR-2796, Nov. 1972.

[20]Moore, F. G., "Aerodynamics of Guided and Unguided Weapons: Part I—Theory and Application," NWL TR-3018, Dec. 1973.

[21]Moore, F. G., Wilcox, F. J., Jr., and Hymer, T.,"Improved Empirical Model for Base Drag Prediction on Missile Configurations Based on New Wind-Tunnel Data," Naval Surface Warfare Center, NSWCDD/TR-92/509, Dahlgren, VA, Oct. 1992.

[22]Jackson, C. M., Jr., Corlett, W. A., and Monta, W. J., "Description and Calibration of the Langley Unitary Plan Wind Tunnel," NASA TP 1905, Nov. 1981.

[23]Braslow, A. L., and Knox, E. C., "Simplified Method for Determination of Critical Height of Distributed Roughness Particles for Boundary-Layer Transition at Mach Numbers from 0 to 5," NACA TN 4363, Sept. 1958.

[24]Braslow, A. L., Hicks, R. M., and Harris, R. V., Jr., "Use of Grit-Type Boundary-Layer-Transition Strips on Wind-Tunnel Models," NASA TN D-3579, Sept. 1966.

[25]Juanarena, D. B., "A Multiport Sensor and Measurement System for Aerospace Pressure Measurements," *Proceedings of the 25th International Instrumentation Symposium*, Anaheim, CA, May 1979.

[26]Butler, C., Sears, E., and Pellas, S., "Aerodynamic Characteristics of 2-, 3-, and 4-Caliber Tangent-Ogive Cylinders with Nose Bluffness Ratios of 0.00, 0.25, 0.50, and 0.75 at Mach Numbers from 0.6 to 4.0," AFATL TR 77-8, Jan. 1977.

[27]Hill, F. K., and Alpher, R. A., "Base Pressure at Supersonic Velocities," Johns Hopkins Univ., Bumblebee Rept. 106, Nov. 1949.